IEEE Access
Multidisciplinary ⋮ Rapid Review ⋮ Open Access Journal

Received 6 July 2024, accepted 20 July 2024, date of publication 29 July 2024, date of current version 8 August 2024.

Digital Object Identifier 10.1109/ACCESS.2024.3434741

RESEARCH ARTICLE

Comparison of Analytical and Algorithm-Based Design of Two-Port Using Two Bilinear Sections

DMITRII SEMENOV[1], ROMAN SOTNER[1], (Member, IEEE), LADISLAV POLAK[1], (Member, IEEE), JAN JERABEK[1], JIRI PETRZELA[1,2], AND LUKAS LANGHAMMER[1,2]

[1]Faculty of Electrical Engineering and Communication, Brno University of Technology, 616 00 Brno, Czech Republic
[2]Faculty of Military Technology, Department of Electrical Engineering, University of Defense, 662 10 Brno, Czech Rrepublic

Corresponding author: Dmitrii Semenov (240689@vut.cz)

This work was supported by Czech Science Foundation under Project 23-06070S.
This work was supported by the institutional support (VAROPS) of the Ministry of Defence of the Czech Republic.

ABSTRACT This paper compares the analytical approach and optimization algorithm for designing a two-bilinear-section-based two-port transfer function hinged on a numerical sweep with the intention of implementing fractional-order (FO) systems in many sensing areas. The study compares analytical and algorithm-based design approaches and tests their effectiveness in designing a two-port system that accommodates phase shifts within the 10° to 80° range and with various phase ripple limits. The impact of phase changes on usable bandwidth (yield maximization) is also explored. The proposed algorithm represents the most optimal approach and calculates zeros/poles frequencies to precisely keep the required mean phase value and phase ripple value for the defined center frequency. Experimental results are provided, utilizing two bilinear sections featuring the current feedback amplifier. Moreover, the implementation of the novel two-port Cole model as an application example of the proposed design is presented and evaluated. The approaches presented are useful in sensing, modeling, and instrumentation.

INDEX TERMS Bilinear section, Cole model, constant phase range, current feedback OPAMP, fractional-order, two-port.

I. INTRODUCTION

Fractional-order behavior, as documented in [1], widens its influence across various domains of human life. Its significance is evident in material studies [2], [3], [4], plant dynamics [5], [6], studies related to biological tissues [7], [8], [9], liquid impedance modeling [10], [11], applications in food sensing [12], [13], and material sensing [14]. Moreover, fractional-order principles find application in conventional electronic systems, including regulators [15], controllers [16], [17], [18], linear filters [19], [20], and oscillators [21].

The FO device [1], also referred to as a constant phase element (CPE) [22], [23], defines a distinct impedance characterized by a flat phase $\varphi_a \in (0, \pm 90°)$, where 0° represents resistor and ±90° represents inductor or capacitor. This element is defined by impedance $Z_a(s) = s^{\pm\alpha} X_a$, where $s^{+\alpha}$ and $X_a = L_a$ are valid for an inductive character, and $s^{-\alpha}$ and $X_a = 1/C_a$ denote a capacitive character. These devices are intentionally designed using solid-state layers of specialized materials [24], liquids [25], and standard lumped resistors and capacitors (RC elements) arranged in ladder structures [22], [23], [26], [27]. These structures create a series of alternating zeros and poles in the symbolical impedance term, defined by subsequently connected serial or parallel RC sections [22], [23]. It's important to note that the operational bandwidth is limited due to the finite number of RC sections, which also affects accuracy (allowed phase ripple). Therefore, the mentioned design approaches provide an approximation of an ideal FO device, which is not physically realizable, as the ideal FO device exhibits a flat phase response across an infinite frequency bandwidth. Some design and modeling

The associate editor coordinating the review of this manuscript and approving it for publication was Sungyong Jung.

tasks necessitate the use of FO two-ports for transfer responses. The impedance formed by the fractional device can be applied directly to special two-port transfer functions or serve as part of an active circuit (e.g. feedback of op-amp or current feedback op-amp) [20]. However, their reconfigurability is usually very limited or requires entirely new values of all RC elements in the ladder. There have been efforts to propose direct electronic configurations for the adjustment of zero and pole locations [28], providing reconfigurability to the device. The first-order transfer block, enabling independent adjustment of zero and pole frequencies, is known as a bilinear section (or segment) [16]. Several examples of such sections have been presented in recent years [29], [30]. As previously mentioned, the number of sections (either bilinear in two ports or RC in impedance) corresponds to the operational bandwidth and phase ripple [22], [23], [31], [32]. A previous study [32] has clearly explained and illustrated this behavior. Many researchers' primary focus is maximizing the FO device's operational frequency range.

A single bilinear section crates a single-phase peak (having a single zero and a single pole). When two bilinear sections are cascaded, they generate two local maximums that can be modified in range and frequency position based on specific requirements. However, there has not been a presented study targeting the optimal location of center frequencies, zeros, and poles of both sections. This work compares two novel methods (analytical and algorithmic search) for the optimal design of a two-section-based FO system. The main goals of this paper include: 1) evaluating bandwidth based on the targeted phase shift, 2) assessing phase ripple on the targeted phase shift, 3) experimentally verifying typical examples of two-section-based operation using standard active elements, and 4) providing an application example of the proposed system of two bilinear sections in a novel Cole two-port suitable for modeling in transfer systems.

We are comparing analytical and algorithm-based approaches in terms of precision and complexity for calculating zeros/poles frequencies for a two-port design. The analytical approach is simple, fast, and evident and can be completed by hand. Conversely, it is less precise than the algorithm-based approach, which requires significantly higher computing power. Moreover, the latter does not provide insight into the design. Another purpose of this paper is to propose methods that are comparable with existing techniques but superior in terms of computational efficiency, alongside an analytical method that requires no computational device. The analytical method offers a manual design approach, which is often not available in similar fractional-order designs, allowing for hand calculations with acceptable trade-offs in operational frequency range and phase ripple balance of the resulting response.

The paper is organized as follows: Section II introduces the parameters of a cascade of bilinear sections in overall and partial phase responses. It explains both design approaches (analytical and algorithm) and compares the obtained results. Section III provides an example of experimental verification and an application example in the novel implementation of a two-port Cole model using standard active elements. Section IV discusses obtained behavior, and Section V concludes this paper.

II. CASCADE OF TWO BILINEAR SECTIONS

The further discussion involves the analysis of two bilinear sections in cascade. The design targets include the center frequency of the cascade, $f_s = 1$ kHz ($\omega_s = 2\pi f_s$), and a phase value (at f_s) of $\varphi_\Sigma = 30°$. The ideal phase ripple is intended to be as minimal as possible $\Delta\varphi_\Sigma \to 0$. The phase ripple is defined as the range of fluctuation around the targeted φ_Σ, i.e., $\varphi_\Sigma \pm \Delta\varphi_\Sigma$. The operational bandwidth is determined by conditions depending on the specific φ_Σ in our case. We consider two bilinear sections, i.e., the operational bandwidth will be within one frequency decade. The cascade of two ideal bilinear sections [32] has a symbolical transfer response $K_s(s)$ in the form:

$$K_s(s) = \left(\frac{s+\omega_{zA}}{s+\omega_{pA}}\right)\cdot\left(\frac{s+\omega_{zB}}{s+\omega_{pB}}\right), \tag{1}$$

where $\omega_{zA,B}$ and $\omega_{pA,B}$ are the real zeros and poles, respectively, of section A and B. The transfer response is shown in Fig. 1 (considered as general for clarification of parameters). It illustrates the magnitude and phase response of resulting transfer of two bilinear sections in cascade (shown in red color). The phase responses of both bilinear sections (A and B, blue color) are also noted for their further importance in the design. The description of section A is provided in form of analytical term and formulas for further utilization in the design. The phase response has the following form [32]:

$$\varphi_A(\omega) = \left[\tan^{-1}\left(\frac{\omega}{\omega_{zA}}\right) - \tan^{-1}\left(\frac{\omega}{\omega_{pA}}\right)\right]. \tag{2}$$

The maximum phase shift $\varphi_A(\omega_A)$ of the section (explained for section A, section B is analogic) at the center frequency ω_A of the section (peak of the blue response) can be expressed

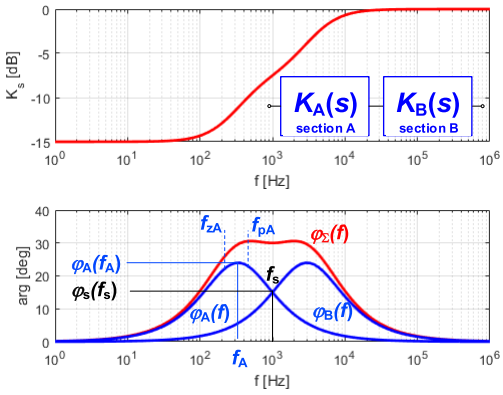

FIGURE 1. General example of frequency response (red color) formed by two bilinear sections.

by the zero ω_{zA} and pole ω_{pA} frequency as:

$$\varphi_A(\omega_A) = \left[\tan^{-1}\left(\frac{\omega_A}{\omega_{zA}}\right) - \tan^{-1}\left(\frac{\omega_A}{\omega_{pA}}\right)\right] = \left[\tan^{-1}\left(\sqrt{\frac{\omega_{pA}}{\omega_{zA}}}\right) - \tan^{-1}\left(\sqrt{\frac{\omega_{zA}}{\omega_{pA}}}\right)\right]. \quad (3)$$

This form can be further simplified when the ratio of pole and zero is considered as $k = \omega_{pA}/\omega_{zA}$:

$$\varphi_A(\omega_A) = \left[\tan^{-1}\left(\sqrt{k}\right) - \tan^{-1}\left(\frac{1}{\sqrt{k}}\right)\right] = \tan^{-1}\left(\frac{k-1}{2\sqrt{k}}\right). \quad (4)$$

Note that the center frequency of section A can be expressed as $\omega_A = \sqrt{(\omega_{zA} \cdot \omega_{pA})}$. The previous derivation results in a direct relation between the maximum phase of section $\varphi_A(\omega_A)$ and the ratio of pole and zero. This ratio k can be expressed from (4) as:

$$k = \tan\left(\frac{\varphi_A(\omega_A)}{2} + \frac{\pi}{4}\right)^2. \quad (5)$$

A. ANALYTICAL APPROACH

The analytical design approach supposes the discussed parameters, resulting in specifications of zeros and poles for bilinear sections. The resulting phase shift is a sum of both responses: $\varphi_\Sigma(\omega) = \varphi_A(\omega) + \varphi_B(\omega)$. The resulting phase $\varphi_\Sigma(\omega_s)$ at the center frequency (f_s) of cascade (both sections) is given by $\varphi_\Sigma(\omega_s) = \varphi_A(\omega_s) + \varphi_B(\omega_s)$, and from Fig. 1 is visible that $\varphi_s(\omega_s) = \varphi_A(\omega_s) = \varphi_B(\omega_s)$; consequently, $\varphi_\Sigma(\omega_s) = 2\varphi_A(\omega_s) = 2\varphi_B(\omega_s) = 2\varphi_s(\omega_s)$.

The calculation of parameters can be divided into several consequent parts: 1) The estimation of the phase value at f_A (f_B respectively). To obtain minimal phase ripple, the sum of phase contributions from $\varphi_A(\omega_A)$ and $\varphi_B(\omega_A)$ at the frequency ω_A, i.e., $\varphi_\Sigma(\omega_A) = \varphi_A(\omega_A) + \varphi_B(\omega_A)$, analogically $\varphi_\Sigma(\omega_B) = \varphi_A(\omega_B) + \varphi_B(\omega_B)$, must be the lowest as possible. It means that $\varphi_A(\omega_A)$ and $\varphi_B(\omega_B)$ must be lower than targeted phase value φ_Σ. The contributions of $\varphi_B(\omega_A)$ and $\varphi_A(\omega_B)$ are small but cannot be omitted. However, there is no possibility to find out the value by simple calculation because features of sections A and B are not known at the beginning of the design. Therefore, some estimation must be provided at this stage: $\varphi_A(\omega_A) = \varphi_\Sigma(\omega_s)/a$. The parameter a represents decreasing coefficient of the phase $\varphi_A(\omega_A)$ compared to $\varphi_\Sigma(\omega_s)$ and can be set empirically considering available phase ripple. For example, a very small phase ripple below 1° results in $a = 1.25$, i.e., $\varphi_A(\omega_A) = 30°/1.25 = 24°$. 2) The next step is the evaluation of required ratio of pole and zero k by (5), i.e. $k = \tan(\varphi_A(\omega_A)/2 + \pi/4)^2 = \tan(24°/2 \cdot \pi/180° + \pi/4)^2 = 2.37$. The phase in the center of operational band allows us to calculate the partial contribution from each section: $\varphi_s(\omega_s) = \varphi_A(\omega_s) = \varphi_B(\omega_s) = \varphi_\Sigma(\omega_s)/2 = 30°/2 = 15°$. 3) The equation for zero frequency ω_{zA} can be established from (2) for ω_s as:

$$\left[\tan^{-1}\left(\frac{\omega_s}{\omega_{zA}}\right) - \tan^{-1}\left(\frac{\omega_s}{k \cdot \omega_{zA}}\right)\right] - \varphi_A(\omega_A) \cdot \frac{\pi}{180} = 0. \quad (6)$$

Because we know values of $\varphi_A(\omega_A) = 24°$, $\varphi_s(\omega_s) = 15°$ and $k = 2.37$, the equation (6) can be solved numerically to obtain $f_{zA} = 217$ Hz (and $f_{zB} = 1.941$ kHz as the second root). The remaining parameters, with the help of $\omega_s = \sqrt{(\omega_A \cdot \omega_B)}$, can be evaluated as: $f_{pA} = f_{zA} \cdot k = 217 \cdot 2.37 = 515$ Hz, $f_A = \sqrt{(f_{zA} \cdot f_{pA})} = \sqrt{(217 \cdot 1.941 \cdot 10^3)} = 334$ Hz, $f_B = f_s^2/f_A = (1 \cdot 10^3)^2/334 = 2.989$ kHz and $f_{pB} = f_{zB} \cdot k = 1.941 \cdot 10^3 \cdot 2.37 = 4.602$ kHz. All these values are valid for characteristics shown in Fig. 1.

B. ALGORITHM-BASED APPROACH

The design target is to develop an algorithm that can calculate frequencies of zeros and poles (f_{pA}, f_{zA}, f_{pB}, f_{zB}) so that phase characteristics are located as close as possible to the user-defined phase ripple range, providing maximum coverage of the user-defined region. The total phase dependence on frequency can be described as a sum of two-phase characteristics with different central frequencies, as given by (2). Using this, the total phase characteristic can be calculated as follows: $\varphi_\Sigma(\omega) = \varphi_A(\omega) + \varphi_B(\omega)$. This form can be rewritten as:

$$\varphi_\Sigma(\omega) = \left[\tan^{-1}\left(\frac{\omega}{\omega_{zA}}\right) - \tan^{-1}\left(\frac{\omega}{k \cdot \omega_{zA}}\right)\right] + \left[\tan^{-1}\left(\frac{\omega}{\omega_{zB}}\right) - \tan^{-1}\left(\frac{\omega}{k \cdot \omega_{zB}}\right)\right]. \quad (7)$$

Differentiating (7) and setting it equal to zero with respect to frequency allows us to find frequency locations of minimum and maximum of the phase characteristic ($\partial\varphi_\Sigma(\omega)/\partial\omega = 0$). The solution of this equation was obtained using Wolfram Alpha [33]. It yielded three roots, where (8) and (9), as shown at the bottom of the page, represent the center frequency of the system and two local maxima (placed symmetrically around center frequency), respectively. The correspondence with the analytical approach is very high. A MATLAB code [42] has been developed for the calculation of zero and poles of each section. The algorithm

$$\omega_s = \sqrt{k \cdot \omega_{zA} \cdot \omega_{zB}} = \sqrt{\omega_{pA} \cdot \omega_{zB}} \quad (8)$$

$$\omega_{A,B} = \sqrt{\frac{1}{2}\left[\pm\sqrt{\left(-\omega_{zA}^2 k + \omega_{zA}\omega_{zB}k^2 + 2\omega_{zA}\omega_{zB}k + \omega_{zA}\omega_{zB} - \omega_{zB}^2 k\right)^2 - 4\left(\omega_{zA}\omega_{zB}k\right)^2} + \omega_{zA}^2 k - \omega_{zA}\omega_{zB}k^2 - 2\omega_{zA}\omega_{zB}k - \omega_{zA}\omega_{zB} + \omega_{zB}^2 k\right]} \quad (9)$$

consists of the following steps: 1) definition of user parameters (center frequency, phase shift, and ripple); 2) sweep of zero/pole frequencies searched $1/1000{\cdot}f_s$ up to $1000{\cdot}f_s$. In each sweep point, three frequencies corresponding to the maximum/minimum phase are calculated using (8) and (9). Phase values are then calculated at these points by (7); and 3) the sum of absolute differences between the calculated phase at these three points and target values (e.g., mean phase $\pm$ ripple) is calculated and set as an objective optimization factor. The resulting parameters that led to the minimum value of the objective factor (bandwidth, f_A, f_B, etc.) are listed, and respective graphs of resulting phase response and swept parameters are plotted.

C. COMPARISON OF BOTH APPROACHES

This section compares the results obtained by both approaches for the same specification ($f_S = 1$ kHz, $\varphi_\Sigma = 30°$). The phase ripple and bandwidth of the phase value within the given limits are the subjects of investigation.

We conducted tests to examine the impact of the analytical parameter a on a phase ripple and operational bandwidth, considering a selected value of φ_Σ phase swept ranging from 10° to 80° (Fig. 2). The phase ripple produced by the algorithm shows no variation since this method maintains this parameter constant in all cases (exactly defined design target). Figure 2(a) highlights the considerable dependence of the bandwidth on φ_Σ from the algorithm-based approach on the targeted phase in comparison with the analytical approach (difference in type of trace). The operational bandwidth is determined by the maximally available phase ripple $\Delta\varphi_\Sigma$ obtained in each specific case of φ_Σ and a. We tested three different values of a: 1.25, 1.21, and 1.15. The phase ripple $\Delta\varphi_\Sigma$ is studied in Fig. 2(b) in all mentioned cases. Based on these experiments, the optimal value for a for high values of φ_Σ and the widest bandwidth requires a modification to $a = 1.15$. However, this value also corresponds to the largest phase ripple. The value $a = 1.21$ appears to be the most optimal for sufficiently acceptable phase ripple (around 1°) while still achieving a good bandwidth (3.5 kHz, valid from 10° up to 60°). On the other hand, a value of $a = 1.25$ results in the narrowest bandwidth (remaining constant up to 50°) and the lowest phase ripple, significantly below 1°.

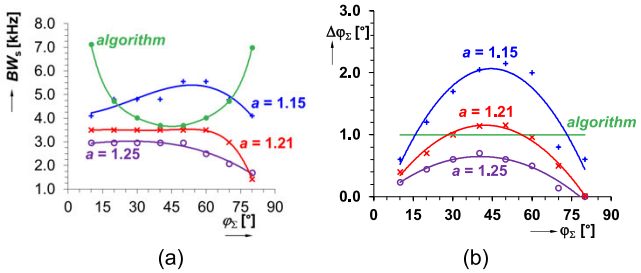

FIGURE 2. Features of the obtained phase response when overall phase shift of cascade of two section is varied: a) operational bandwidth, b) phase ripple.

To conclude, bandwidth can be adjusted and optimized in analytical approach (by a) while it strongly depends on φ_Σ phase and phase ripple $\Delta\varphi_\Sigma$ values in algorithm.

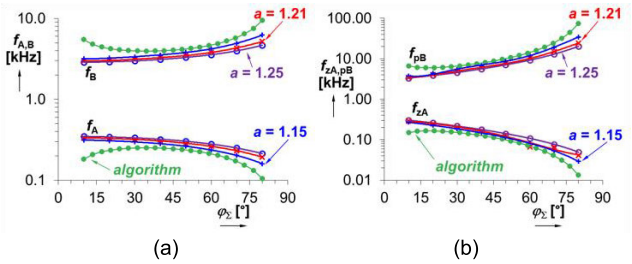

FIGURE 3. Dependences of important frequencies on overall phase response of cascade for: a) variation of center frequencies of sections, b) first zero and last pole frequencies.

As visible in Fig. 3, the center frequencies of bilinear sections A and B exhibit an increasing distance from each other as φ_Σ increases. The same trend is observed for the first zero f_{zA} and last pole f_{pB} frequencies. The algorithm-based results are shown in green, while analytical results are represented with indicated value of parameters a. Results in Fig. 4 show the general trend of increased bandwidth with increased phase ripple. Fig. 5 shows the dependence of the bandwidth on the targeted phase, with the phase ripple set constant $\Delta\varphi_\Sigma = 10°$ in all tested cases. The resulting bandwidth initially decreases with the setting of phase φ_Σ up to 45°; afterward, it increases again. This behavior can be attributed to the trend of a frequency difference between the two maximum peaks (see Fig. 5(b)) of sections, presented in Fig. 6(c).

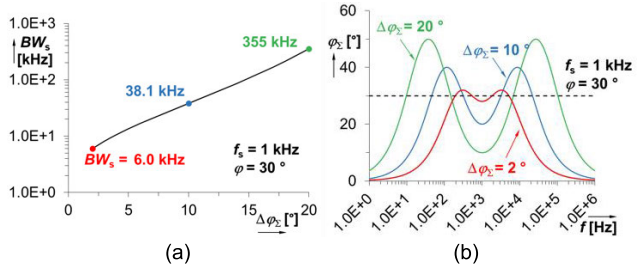

FIGURE 4. Dependence of bandwidth on targeted phase ripple value (algorithm): a) nomogram, b) example of behavior for three selected phase ripples.

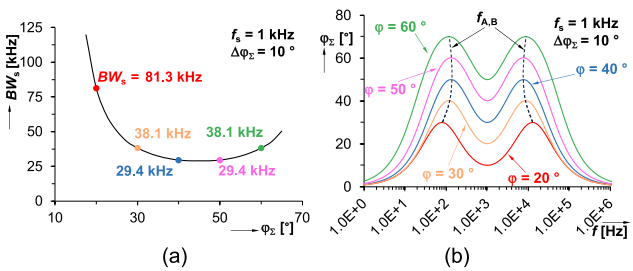

FIGURE 5. Dependence of bandwidth on targeted phase value (algorithm): a) nomogram, b) example of behavior for several selected phases with a highlight of maximum peak frequencies.

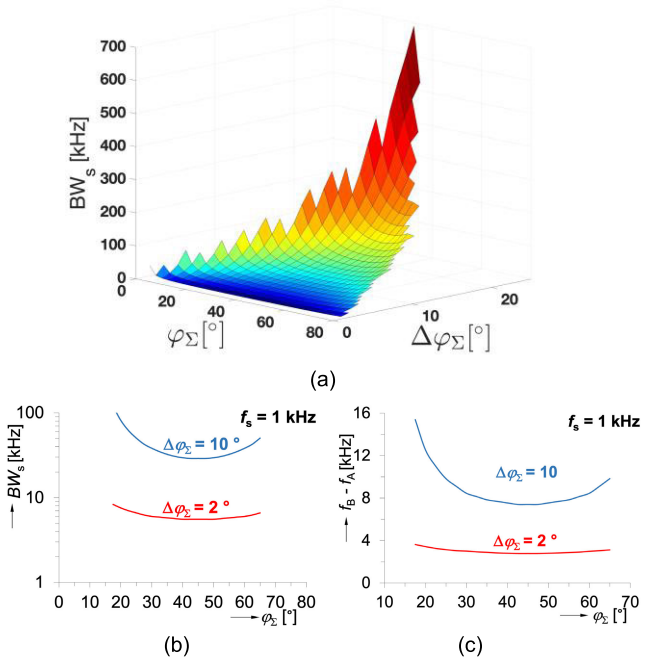

FIGURE 6. The bandwidth evaluation for phase shift and phase ripple (algorithm): a) 3D plot, b) example for two ripples in 2D plot. c) The difference between phase maximum peaks for two ripples.

For both phase ripple values, the smallest frequency difference is observed at 45°, leading to the smallest bandwidth at this phase value. The 3D plot in Fig. 6 visually depicts the simultaneous effects of the targeted phase, bandwidth, and phase ripple. These results clearly confirm an increase in bandwidth with an increase in phase ripple. The narrowest bandwidth with a fixed phase ripple is obtained for $\varphi_\Sigma = 45°$ in all cases.

III. EXPERIMENTAL VERIFICATION

A. TWO-PORT USING TWO BILINEAR SECTIONS

The topology in Fig. 7, consisting of two bilinear sections, was established for experimental tests using two AD844 current feedback operational amplifiers (CFOAs).

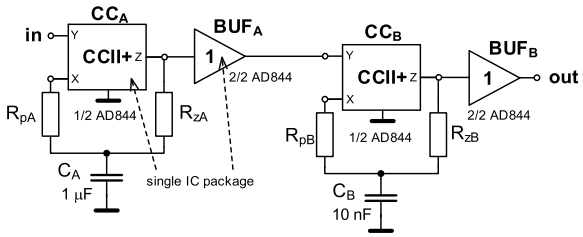

FIGURE 7. Circuit topology used for experimental verification.

This circuit has the transfer function:

$$K_s(s) = \left(\frac{sC_AR_{zA}+2}{sC_AR_{pA}+2}\right)\cdot\left(\frac{sC_BR_{zB}+2}{sC_BR_{pB}+2}\right), \qquad (10)$$

as described in [29]. The features discussed in the previous section were obtained using the presented algorithm

TABLE 1. Resistance values for different sets of phase.

φ_Σ	$\Delta\varphi_\Sigma$	R_{pA}	R_{zA}	R_{pB}	R_{zB}
20°		2.39 kΩ	7.06 kΩ	1.44 kΩ	4.24 kΩ
30°	10°	137 Ω	599 Ω	169 Ω	738 Ω
60°		648 Ω	15.8 kΩ	641 Ω	15.6 kΩ

($f_s = 1$ kHz, $\varphi_\Sigma = 30°$, $\Delta\varphi_\Sigma = 2°$, 10°, and 20°). The capacitor values were chosen to optimize the expected operational bandwidth: $C_A = 1$ µF, $C_B = 10$ nF. Then, the values of resistors were computed for $\Delta\varphi_\Sigma = 10°$ and presented in Table 1. The Keysight DSO-X 3022T oscilloscope with Frequency Response Analysis (FRA) function was used for measurements. The block scheme of the measurement principle is shown in Fig. 8. The input of the tested circuit was connected to the first channel (CH1) and the internal generator (needed for automatic FRA measurement). The input amplitude of a signal was set to 100 mV, and the phase response was measured in a frequency range of 10 Hz - 1 MHz (an oscilloscope frequency range limits lower bound). The output of the circuit was connected to the second channel (CH2) with further phase calculation using an internal measurement function. The experimental workspace is shown in the Fig. 9.

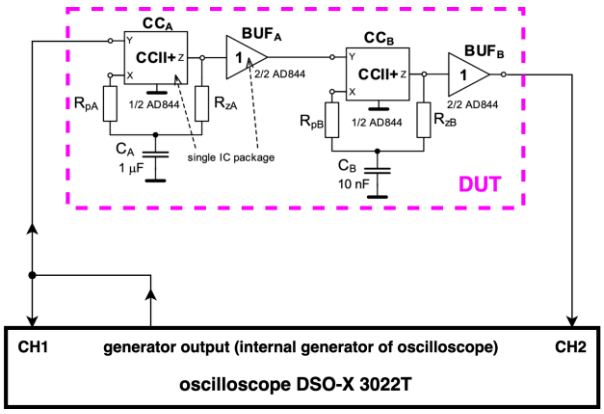

FIGURE 8. Principle of measurement of frequency response.

The measurement results are shown in Fig. 10 and compared with ideal expectations. The experimental verification was made for points $\varphi_\Sigma = 20°$, 30° and 60° to cover the entire range of phase value. The phase ripple variation is tested for $\varphi_\Sigma = 30°$ (see in Fig. 11) with the same capacitor values $C_A = 1$ µF, $C_B = 10$ nF and the resistance parameters listed in Table 2. For Fig. 10(b), Fig. 10(c) and Fig. 11(b), Fig. 11(c) only two datasets with the smallest and highest parameter values were plotted for visual inspection.

The experimental verification was conducted for points $\Delta\varphi_\Sigma = 2°$, 10° and 20°. In one case, the bandwidth had to be estimated because it was partly out of the bandwidth of the measuring equipment. Particularly for $\Delta\varphi_\Sigma = 20°$, the bandwidth value was predicted based on the symmetry of the

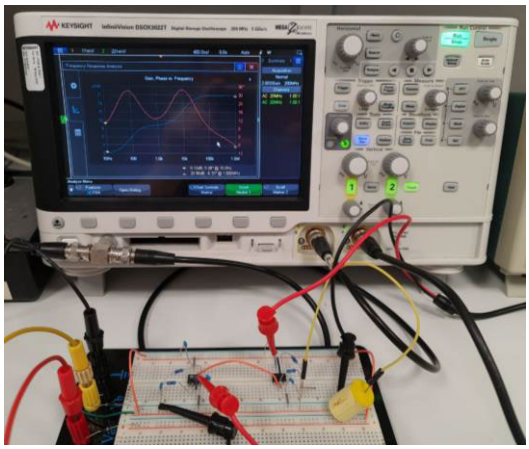

FIGURE 9. Experimental workplace with the constructed protoboard and FRA analysis mode on the oscilloscope DSO-X 3022T.

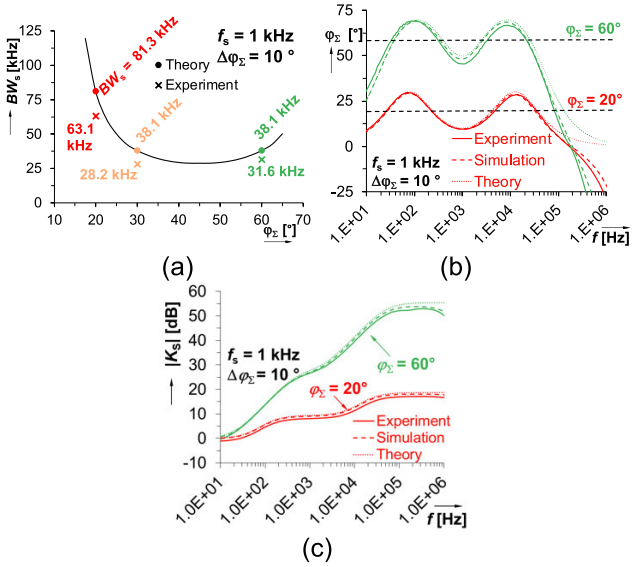

FIGURE 10. The dependencies on the phase value: a) nomogram of bandwidth, b) phase responses, and c) magnitude responses for two selected phase shifts.

TABLE 2. Resistance values for different sets of ripple.

φ_Σ	$\Delta\varphi_\Sigma$	R_{pA}	R_{zA}	R_{pB}	R_{zB}
30°	2°	764 Ω	2.1 kΩ	482 Ω	1.33 kΩ
	10°	137 Ω	599 Ω	169 Ω	738 Ω
	20°	315 Ω	2.35 kΩ	431 Ω	3.22 kΩ

operational band around the center frequency and the right part of the characteristics (the oscilloscope range limitation is 10 Hz). The experimental results closely align with simulations, showing differences in percentage units. However, discrepancies in high-frequency behavior are evident in phase responses, influenced by additional parasitic elements such as stray capacitances on the PCB.

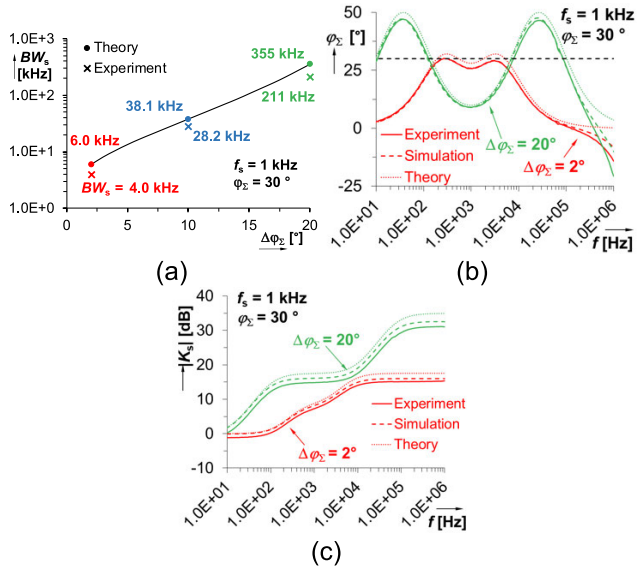

FIGURE 11. The dependencies on the phase ripple value: a) nomogram of bandwidth, b) phase responses, and c) magnitude responses for two selected phase ripples.

B. SENSITIVITY ANALYSIS OF THE CIRCUIT

The relative sensitivity of all component values (R_{zA}, R_{pA}, C_A, R_{zB}, R_{pB}, C_B) of the circuit, presented in Fig. 7, was evaluated with respect to the frequency of zero and pole. In general, the relative sensitivity can be defined as:

$$S_{R,x} = \frac{\Delta y/y}{\Delta x/x} = \frac{\partial y}{\partial x} \cdot \frac{x}{y}, \tag{11}$$

where y is the observed parameter of the two port (zero/pole frequency in this case), and x is the circuit element parameter/value (which variation impacts the function). Considering the magnitude function of the two-section case of the proposed scheme (10), the zero frequency of each section can be defined as $f_{zi} = 2/C_i R_{zi}$, and the pole frequency $f_{pi} = 2/C_i R_{pi}$, for $i = A, B, \ldots$. The relative sensitivity (for R_{pA}, for example) of the pole frequency can be evaluated as $S_{R,RpA} = [-2/C_A R_{pA}^2] \cdot [R_{pA}/(2/C_A R_{pA})] = -1$. Here, the first term $[-2/C_A R_{pA}^2]$ is the derivative of the pole frequency with respect to R_{pA}, and the second term $[R_{pA}/(2/C_A R_{pA})]$ is the circuit element parameter R_{pA} divided by the pole frequency. Consequently, all relative sensitivities of zero and pole frequencies can be obtained for each circuit parameter. The results are presented in Table 3.

TABLE 3. Relative sensitivity values for two-section bilinear circuit.

parameter	R_{pA}	R_{zA}	C_A	R_{pB}	R_{zB}	C_B
f_{zA}	0	−1	−1	0	0	0
f_{pA}	−1	0	−1	0	0	0
f_{zB}	0	0	0	0	−1	−1
f_{pB}	0	0	0	−1	0	−1

C. COLE TWO-PORT MODEL

The previously described approaches to the design of a constant phase device can be applied to the so-called Cole impedance model [34]. Recently, researchers have defined numerous situations involving materials, biological entities, mechanical systems, etc., where this model is significant for providing real and accurate behavioral descriptions [35], [36], [37], [38], [39]. Its importance is particularly notable in sensing applications based on electrical impedance spectroscopy [40]. However, the Cole impedance model characterizes the impedance of the system. Our focus and intention are directed towards developing a new transfer model better suited for describing the signal transfer response of a two-port system, with clear definitions of input and output. Such a model may offer useful features for investigating external influences, signal variations, etc., compared to a simple impedance model. Additionally, it is well-suited for signal processing and control purposes. The Cole impedance model is shown in Fig. 12, and its impedance can be expressed as:

$$Z_{cole}(s) = R_\infty + \frac{1}{s^\alpha C_\alpha + G_P}, \tag{12}$$

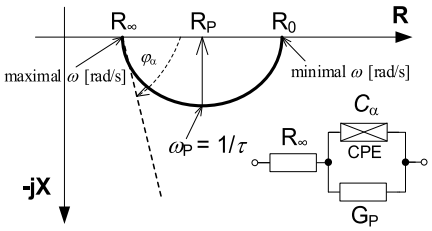

FIGURE 12. The Cole impedance model [11] used for biological, material and tissue representation.

where the parallel resistor R_P is expressed as the conductivity G_P for better correspondence with the following explanations. In general, there are two possibilities for creating a two-port Cole model. The first solution, as it is shown in Fig. 13(a), implements the Cole impedance as the feedback impedance of an operational amplifier (OA) or a current conveyor of second generation (CCII) [41]. The transfer response of the OA-based concept has the form of $K_{\text{cole}}(s) = -Z_{\text{cole}}(s)/R_{\text{ref}} = -1/R_{\text{ref}} \cdot (R_\infty + 1/(s^\alpha C_\alpha + G_p))$, where parameters can be interpreted as $K_\infty = R_\infty/R_{\text{ref}}$, $D_\alpha = C_\alpha \cdot R_{\text{ref}}$, $K_p = G_p \cdot R_{\text{ref}} = R_{\text{ref}}/R_p$. The same equation is valid for CCII, except for the negative polarity (CCII has a noninverting character) of the transfer. The second solution in Fig. 13(b) benefits from the simple possibility of adjusting each parameter of the model electronically, as shown in its transfer response:

$$K_{cole}(s) = K_\infty + \frac{1}{s^\alpha D_\alpha + K_P}. \tag{13}$$

The application example assumes a specific slope of phase (linear increase of 3° with frequency) in a single decade from 200 Hz up to 2 kHz. Note that this behavior (smooth phase slope settings) cannot be easily obtained in integer-order systems and without Cole model. The parameters of the model in Fig. 13(b) are as follows: $K_\infty = 3$, $K_P = 0.01$, $D_\alpha = 0.15$, $\alpha = 0.33$ ($\varphi_\Sigma = 30°$, $\Delta\varphi_\Sigma = 2°$ from the previous test, see Fig. 11). The amplifiers K_∞ and K_P are implemented using an inverting amplifier with OA TL072, summing operation by AD830 and a differentiator by the circuit in Fig. 7 connected in negative feedback of OA TL072. The single-decade operation can be easily approximated by the proposed two-bilinear section-based system on abovementioned Cole model. The operational range is defined by a maximal phase error up to 10% from 130 Hz up to 5.5 kHz. The magnitude, phase response and Nyquist plot are shown in Fig. 14. The notable differences between the simulated and theoretical traces are caused by the limited applicability of the Cole model, which employs only two sections for approximating the fractional-order differentiator.

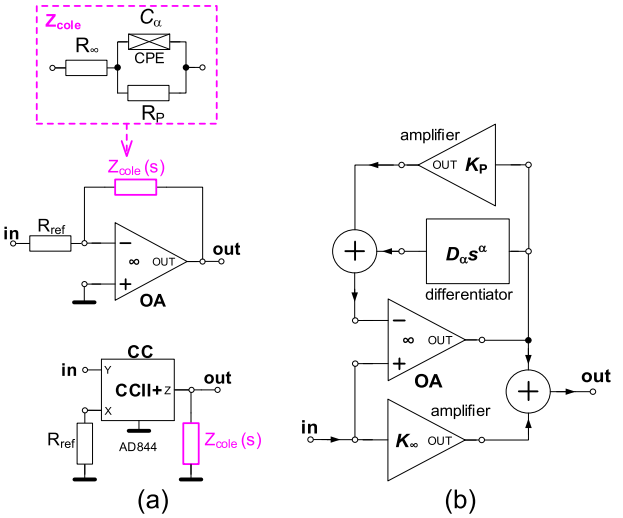

FIGURE 13. The Cole two-port model: a) based on Cole impedance, b) utilizing complete signal processing operations.

IV. DISCUSSION

The analytical approach limits the maximum phase ripple, directly influencing the intended bandwidth. As shown, the value of the empirical coefficient a is crucial for both ripple and bandwidth. The almost constant phase ripple (around 1-1.2°) is achieved with the optimal a value of 1.21, ensuring a consistently flat bandwidth of 3.5 kHz from 10° up to 60°. The minimal phase ripple occurs at the low and high corners of the targeted phase value (below 15° and above 70°), while the maximal ripple is observed around 45°. The analytical approach provides empirical flexibility (through parameter a) for manual bandwidth optimization (extension). However, determining the optimal value for parameter a requires the designer's experience and multiple design simulations.

The algorithmic approach adapts the phase ripple to the required bandwidth for all selected phase shifts. This means

TABLE 4. Comparison of the existing solutions.

Study	Method	Base approach*	Precision	Flexibility	Computational Efficiency	Time of design	Sensitivity analysis	Structure	Control method
[20]	Analytical and optimization	Analytical, algorithm	Depends on optimization	High	Moderate	Few seconds	Monte Carlo included[1]	2x CFOA	R, C values
[43]	Bilinear Double-Order Filter	Algorithm	High	Moderate	Moderate	Few seconds	Monte Carlo included[2]	RC ladder, 2x CFOA	R, C values
[44]	RC ladder approximation	Analytical	High	Moderate	Low	Few minutes	Not included	RC ladder	R, C values
[45]	Curve fitting approximation	Algorithm	High	High	High	Few seconds	Monte Carlo included[3]	FLF structure with OTAs	OTA g_m values
[46]	Matrix method	Analytical	Moderate	High	Low	Few minutes	Not included	4x OTA or 1x DVCC	OTA g_m values
This work	Analytical	Analytical	Moderate	Moderate	Low	Few minutes	Included	2x CFOA (AD844)	R, C values
This work	Algorithm-based	Algorithm	High	High	High	Few seconds	Included	2x CFOA (AD844)	R, C values

CFOA - current feedback operational amplifier; DVCC - differencing voltage current conveyor; FLF - follow the leader feedback; OTA - operational transconductance amplifier; g_m - transconductance parameter of OTA;
* - "analytical" approach needs no computational device while "algorithm" does
[1] - the frequency standard deviation is 2.2% from the mean value for low-pass filter and 4.4% from the mean for band-pass filter;
[2] - the frequency standard deviation is 2.3% for two proposed double-order compensators compared to the mean values;
[3] - the frequency standard deviation is 10.2% from the mean value for low-pass filter and 1.6% from the mean for band-pass filter

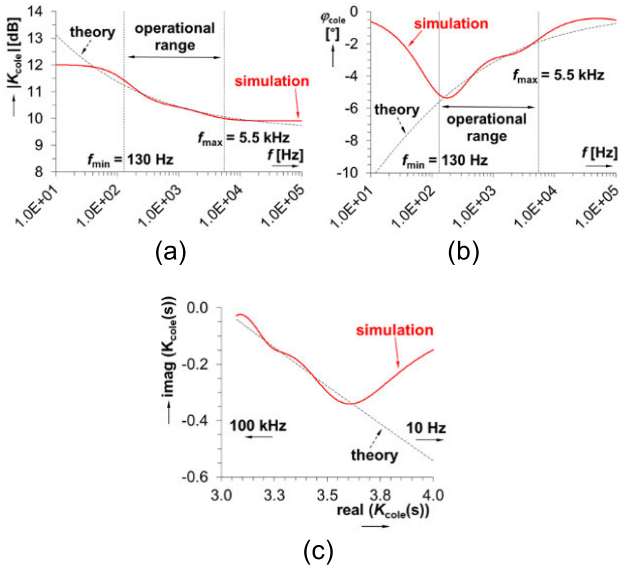

FIGURE 14. Analysis of the Cole two-port model: a) magnitude response, b) phase response, and c) Nyquist plot.

that a high-phase ripple allows for the design of a wide-band response and vice versa. Therefore, a requirement for a very small phase ripple decreases operational bandwidth. Although the algorithmic approach results in a constant phase ripple, it also leads to a variation in bandwidth (decreasing with increasing phase). However, the function has a local minimum, after which the bandwidth increases again. The decrease of phase ripple $\Delta\varphi_\Sigma$ for identical phase value φ_Σ means decrease of bandwidth. Both approaches have a theoretical calculation limit of usability up to $\varphi_\Sigma = 90°$ due to overlapping locations of zeros and poles. To keep the feature of a constant-phase element with a fixed ripple value, zeros and poles should alternate between each other. This theoretical maximum phase value is limited to 90°. In practice, the mean phase limitation is also defined by the phase ripple, so their sum $(\varphi_\Sigma + \Delta\varphi_\Sigma)$ cannot exceed 90°. Additionally, the algorithm-based approach has a limit on maximal phase ripple, up to $\Delta\varphi_\Sigma = 25°$, which was obtained by sweeping phase ripple values and evaluating parameters at each point. A comparison between both proposed solutions and already existing solutions is presented in Table 4. There, an algorithm-based approach shows decent performance and stands as one of the best available methods for cascades of bilinear sections design in terms.

For both approaches, a general recommendation can be defined: if the widest BW is required, the maximum possible phase ripple should be set with the minimum mean phase. This can be clearly seen in Fig. 4(a) and Fig. 5(a) for algorithm-based approach and in Fig. 3 for analytical-based.

V. CONCLUSION

A. APPROACHES HIGHTLIGHTS

The presented results highlight the advantages of a two bilinear section (two real zeros and two real poles) -based two-port in designing for more than one frequency decade validity of a constant phase range, tested between 10° and 80° with various phase ripples. The analytical approach yields very low and flat phase ripple (up to 2°) dependence on the target phase value, while the bandwidth (3-5 kHz) does not

significantly change up to 60° of the targeted phase value. The phase ripple changes within a certain range, from very low values around the low and high corners of targeted phase values (below 15° and above 70°) to a maximum of around 45°. On the other hand, the algorithm operates with a constant phase ripple in any case, resulting in a significant bandwidth variation (4-7 kHz). The phase ripple is constant across the full operational frequency range and for all targeted phase values. The bandwidth dependence on the targeted phase has a minimum in the middle (45°) of the tested range. Based on the observed behavior, the analytical approach provides the widest frequency operational range for many targeted phase values. In addition, the design parameters can be calculated in a simple, straightforward way without the necessity of an algorithm using iteration cycles (are required, for example, in [22] and [32]), which was the goal of its proposal. However, some estimation is required based on the designer's judgment and experience (i.e., parameter a). On the other hand, the algorithm here provides a more exact solution based on the most optimal automatic numerical design of zero/poles locations (by least square method) for two-section-based examples than the analytical approach. The more precise result for two sections (in bandwidth and ripple) is also obtained here compared to the typical method presented in [22].

B. ALGORITHM-BASED APPROACH APPLICATION

The proposed algorithm effectively and precisely designs bilinear sections by specifying the central frequency, phase mean value, and phase ripple value. The proposed method is suitable for the design of fractional order two-ports, filters, and impedances of specific purpose [15], [16], [17], [18], [19], [20], [21]. It can also be used by designers of fractional-order circuits for a quick calculation of zero/poles frequencies of two sections in a cascade. The proposed two-port structure is applied to design a novel Cole model to evaluate two-port signal operations. The transfer response instead of impedance can offer advantages in various modeling situations.

C. LIMITATIONS AND CONSTRAINTS

The algorithm-based approach, while highly precise, can be inefficient due to the significant computational and processing power it requires. Additionally, this approach necessitates input data (mean and ripple phase values) within a specific range, as shown in Fig. 6(a). The sum of the phase ripple and mean value would not exceed 90°, and their difference should be positive. The current algorithm and analytical-based approach assume two bilinear-section structures, limiting the constant-phase operating range. Furthermore, approximating more complex models, such as the transmission-line circuit (which consists of LC components and is a second-order system), is not feasible with the proposed approaches, as they require more sections with complex roots (more complex zero/poles) than those used in this work.

In conclusion, the algorithm-based approach should be employed in designing systems where accuracy is the most crucial parameter. In contrast, the analytical-based approach, though less effective and accurate, can be used for calculations without a computational device, making it preferable when computational resources are limited.

REFERENCES

[1] A. S. Elwakil, "Fractional-order circuits and systems: An emerging interdisciplinary research area," *IEEE Circuits Syst. Mag.*, vol. 10, no. 4, pp. 40–50, Sep. 2010, doi: 10.1109/MCAS.2010.938637.

[2] L. Su, J. Muñoz-Enano, P. Vélez, P. Casacuberta, M. Gil, and F. Martín, "Phase-variation microwave sensor for permittivity measurements based on a high-impedance half-wavelength transmission line," *IEEE Sensors J.*, vol. 21, no. 9, pp. 10647–10656, May 2021, doi: 10.1109/JSEN.2021.3063112.

[3] M. Aleksandrova, "Characterization of infrared detector with lead-free perovskite and core–shell quantum dots on silicon substrate," *J. Mater. Sci. Mater. Electron.*, vol. 33, no. 31, pp. 23900–23909, Nov. 2022, doi: 10.1007/s10854-021-07339-7.

[4] L. Zhang, S. Chang, X. Lu, T. Han, R. Jin, T. Zhao, D. Fang, M. Xie, M. Wang, and J. Yi, "Vapor phosphorus-coated cobalt vanadate as a high-performance anode for a lithium-ion battery," *J. Solid State Electrochemistry*, vol. 26, no. 4, pp. 917–927, Apr. 2022, doi: 10.1007/s10008-022-05127-9.

[5] J.-J. Cabrera-López and J. Velasco-Medina, "Structured approach and impedance spectroscopy microsystem for fractional-order electrical characterization of vegetable tissues," *IEEE Trans. Instrum. Meas.*, vol. 69, no. 2, pp. 469–478, Feb. 2020, doi: 10.1109/TIM.2019.2904131.

[6] S. Kapoulea, C. Psychalinos, and A. S. Elwakil, "Realization of cole-Davidson function-based impedance models: Application on plant tissues," *Fractal Fractional*, vol. 4, no. 4, p. 54, Nov. 2020, doi: 10.3390/fractalfract4040054.

[7] A. Prasad and M. Roy, "Bioimpedance analysis of vascular tissue and fluid flow in human and plant body: A review," *Biosystems Eng.*, vol. 197, pp. 170–187, Sep. 2020, doi: 10.1016/j.biosystemseng.2020.06.006.

[8] D. A. Yousri, A. M. Abdelaty, L. A. Said, A. AboBakr, and A. G. Radwan, "Biological inspired optimization algorithms for cole-impedance parameters identification," *Int. J. Electron. Commun.*, vol. 78, pp. 79–89, Aug. 2017, doi: 10.1016/j.aeue.2017.05.010.

[9] B. Fu and T. J. Freeborn, "Cole-impedance parameters representing biceps tissue bioimpedance in healthy adults and their alterations following eccentric exercise," *J. Adv. Res.*, vol. 25, pp. 285–293, Sep. 2020, doi: 10.1016/j.jare.2020.05.016.

[10] Md. E. E. E. Alahi, N. Pereira-Ishak, S. C. Mukhopadhyay, and L. Burkitt, "An Internet-of-Things enabled smart sensing system for nitrate monitoring," *IEEE Internet Things J.*, vol. 5, no. 6, pp. 4409–4417, Dec. 2018, doi: 10.1109/JIOT.2018.2809669.

[11] J. Slay, R. Sotner, T. J. Freeborn, J. Jerabek, L. Polak, J. Petrzela, and V. Vyplel, "Distinguishing liquid solutions with alcohol using electrical impedance measurements: Preliminary study for food safety applications," *IEEE Sensors J.*, vol. 23, no. 22, pp. 26997–27007, Nov. 2023, doi: 10.1109/JSEN.2023.3315798.

[12] H. Jiang, M. Zhang, B. Bhandari, and B. Adhikari, "Application of electronic tongue for fresh foods quality evaluation: A review," *Food Rev. Int.*, vol. 34, no. 8, pp. 746–769, Jan. 2018, doi: 10.1080/87559129.2018.1424184.

[13] J. Tan and J. Xu, "Applications of electronic nose (e-nose) and electronic tongue (e-tongue) in food quality-related properties determination: A review," *Artif. Intell. Agricult.*, vol. 4, pp. 104–115, Jun. 2020, doi: 10.1016/j.aiia.2020.06.003.

[14] I. Piekarz, J. Sorocki, K. Wincza, and S. Gruszczynski, "Liquids permittivity measurement using two-wire transmission line sensor," *IEEE Sensors J.*, vol. 18, no. 18, pp. 7458–7466, Sep. 2018, doi: 10.1109/JSEN.2018.2856889.

[15] L. Kadlcík and P. Horský, "A CMOS follower-type voltage regulator with a distributed-element fractional-order control," *IEEE Trans. Circuits Syst. I, Reg. Papers*, vol. 65, no. 9, pp. 2753–2763, Sep. 2018, doi: 10.1109/TCSI.2018.2808879.

[16] P. Chen and Y. Luo, "Analytical fractional-order PID controller design with Bode's ideal cutoff filter for PMSM speed servo system," *IEEE Trans. Ind. Electron.*, vol. 70, no. 2, pp. 1783–1793, Feb. 2023, doi: 10.1109/TIE.2022.3158009.

[17] M. F. Tolba, L. A. Said, A. H. Madian, and A. G. Radwan, "FPGA implementation of the fractional order Integrator/differentiator: Two approaches and applications," *IEEE Trans. Circuits Syst. I, Reg. Papers*, vol. 66, no. 4, pp. 1484–1495, Apr. 2019, doi: 10.1109/TCSI.2018.2885013.

[18] J. Nako, C. Psychalinos, and A. S. Elwakil, "Minimum active component count design of a PIλDμ controller and its application in a cardiac pacemaker system," *J. Low Power Electron. Appl.*, vol. 13, no. 1, p. 13, Feb. 2023, doi: 10.3390/jlpea13010013.

[19] O. Domansky, R. Sotner, L. Langhammer, and L. Polak, "Electronically reconfigurable and tunable fractional-order filter using resonator concept and feedforward path for low-frequency tone signalization," *IEEE Access*, vol. 9, pp. 138026–138041, 2021, doi: 10.1109/ACCESS.2021.3118084.

[20] J. Nako, C. Psychalinos, A. S. Elwakil, and S. Minaei, "Non-integer order generalized filters designs," *IEEE Access*, vol. 11, pp. 116846–116859, 2023, doi: 10.1109/ACCESS.2023.3325911.

[21] R. Sotner, J. Jerabek, L. Polak, L. Langhammer, H. Stolarova, J. Petrzela, D. Andriukaitis, and A. Valinevicius, "On the performance of electronically tunable fractional-order oscillator using grounded resonator concept," *Int. J. Electron. Commun.*, vol. 129, Feb. 2021, Art. no. 153540, doi: 10.1016/j.aeue.2020.153540.

[22] J. Valsa, P. Dvork, and M. Friedl, "Network model of the CPE," *Radioengineering*, vol. 20, no. 3, pp. 619–626, 2011.

[23] J. Valsa and J. Vlach, "RC models of a constant phase element," *Int. J. Circuit Theory Appl.*, vol. 41, no. 1, pp. 59–67, Jan. 2013, doi: 10.1002/cta.785.

[24] P. Ushakov, A. Shadrin, D. Kubanek, and J. Koton, "Passive fractional-order components based on resistive-capacitive circuits with distributed parameters," in *Proc. 39th Int. Conf. Telecommun. Signal Process. (TSP)*, Jun. 2016, pp. 638–642, doi: 10.1109/TSP.2016.7760960.

[25] A. Adhikary, M. Khanra, S. Sen, and K. Biswas, "Realization of a carbon nanotube based electrochemical fractor," in *Proc. IEEE Int. Symp. Circuits Syst. (ISCAS)*, May 2015, pp. 2329–2332, doi: 10.1109/ISCAS.2015.7169150.

[26] A. Adhikary, S. Sen, and K. Biswas, "Practical realization of tunable fractional order parallel resonator and fractional order filters," *IEEE Trans. Circuits Syst. I, Reg. Papers*, vol. 63, no. 8, pp. 1142–1151, Aug. 2016, doi: 10.1109/TCSI.2016.2568262.

[27] A. Adhikary, S. Choudhary, and S. Sen, "Optimal design for realizing a grounded fractional order inductor using GIC," *IEEE Trans. Circuits Syst. I, Reg. Papers*, vol. 65, no. 8, pp. 2411–2421, Aug. 2018, doi: 10.1109/TCSI.2017.2787464.

[28] R. Sotner, J. Jerabek, J. Petrzela, O. Domansky, G. Tsirimokou, and C. Psychalinos, "Synthesis and design of constant phase elements based on the multiplication of electronically controllable bilinear immittances in practice," *Int. J. Electron. Commun.*, vol. 78, pp. 98–113, Aug. 2017, doi: 10.1016/j.aeue.2017.05.013.

[29] R. Sotner, J. Petrzela, O. Domansky, and T. Dostal, "Current feedback operational amplifier based two-port frequency equalizer," in *Proc. Eur. Conf. Circuit Theory Design (ECCTD)*, Sep. 2017, pp. 1–4, doi: 10.1109/ECCTD.2017.8093278.

[30] R. Sotner, L. Polak, J. Jerabek, and J. Petrzela, "Simple two operational transconductance amplifiers-based electronically controllable bilinear two port for fractional-order synthesis," *Electron. Lett.*, vol. 54, no. 20, pp. 1164–1166, Oct. 2018, doi: 10.1049/el.2018.5575.

[31] N. Mijat, D. Jurisic, and G. S. Moschytz, "Analog modeling of fractional-order elements: A classical circuit theory approach," *IEEE Access*, vol. 9, pp. 110309–110331, 2021, doi: 10.1109/ACCESS.2021.3101160.

[32] P. Prommee and P. Pienpichayapong, "Reconfigurable fractional-order operator and bandwidth expansion suitable for PIa controller," *IEEE Trans. Ind. Electron.*, vol. 71, no. 5, pp. 1–11, Aug. 2023, doi: 10.1109/TIE.2023.3288170.

[33] *Wolfram Alpha*, Wolfram Alpha LLC, Champaign, IL, USA, 2016.

[34] K. S. Cole, "Permeability and impermeability of cell membranes for ions," in *Proc. Cold Spring Harbor Symp. Quantitative Biology*, vol. 8, Jan. 1940, pp. 110–122.

[35] T. J. Freeborn, "A survey of fractional-order circuit models for biology and biomedicine," *IEEE J. Emerg. Sel. Topics Circuits Syst.*, vol. 3, no. 3, pp. 416–424, Sep. 2013, doi: 10.1109/JETCAS.2013.2265797.

[36] T. J. Freeborn, B. Maundy, and A. S. Elwakil, "Extracting the parameters of the double-dispersion Cole bioimpedance model from magnitude response measurements," *Med. Biol. Eng. Comput.*, vol. 52, no. 9, pp. 749–758, Sep. 2014, doi: 10.1007/s11517-014-1175-5.

[37] T. J. Freeborn, A. S. Elwakil, and B. Maundy, "Variability of cole-model bioimpedance parameters using magnitude-only measurements of apples from a two-electrode configuration," *Int. J. Food Properties*, vol. 20, no. 1, pp. S507–S519, Dec. 2017, doi: 10.1080/10942912.2017.1300810.

[38] C. Vastarouchas, G. Tsirimokou, and C. Psychalinos, "Extraction of cole-cole model parameters through low-frequency measurements," *Int. J. Electron. Commun.*, vol. 84, pp. 355–359, Feb. 2018, doi: 10.1016/j.aeue.2017.11.020.

[39] C. Vastarouchas, C. Psychalinos, A. S. Elwakil, and A. A. Al-Ali, "Novel two-measurements-only cole-cole bio-impedance parameters extraction technique," *Measurement*, vol. 131, pp. 394–399, Jan. 2019, doi: 10.1016/j.measurement.2018.09.008.

[40] L. A. Buscaglia, O. N. Oliveira, and J. P. Carmo, "Roadmap for electrical impedance spectroscopy for sensing: A tutorial," *IEEE Sensors J.*, vol. 21, no. 20, pp. 22246–22257, Oct. 2021, doi: 10.1109/JSEN.2021.3085237.

[41] E. Yuce and S. Minaei, *Passive and Active Circuits By Example*. Cham, Switzerland: Springer, Nov. 2023.

[42] (2024). *Bilinear-paper Repository With Appendix Codes on GitFront*. Accessed: Feb. 4, 2024. [Online]. Available: https://gitfront.io/r/evvejiji/CC7G67a45xEE/bilinear-paper/

[43] J. Nako, C. Psychalinos, F. Khateb, and A. S. Elwakil, "Bilinear double-order filter designs and application examples," *IEEE Access*, vol. 12, pp. 14040–14049, 2024, doi: 10.1109/ACCESS.2024.3357092.

[44] J. Petrzela, "Arbitrary phase shifters with decreasing phase," in *Proc. 38th Int. Conf. Telecommun. Signal Process. (TSP)*, Jul. 2015, pp. 682–686, doi: 10.1109/tsp.2015.7296350.

[45] J. Nako, C. Psychalinos, A. S. Elwakil, and D. Jurisic, "Design of higher-order fractional filters with fully controllable frequency characteristics," *IEEE Access*, vol. 11, pp. 43205–43215, 2023, doi: 10.1109/ACCESS.2023.3271863.

[46] J. Petrzela, "Bilinear reconfigurable filters derived by using matrix method of unknown nodal voltages," in *Proc. 38th Int. Conf. Telecommun. Signal Process. (TSP)*, Jul. 2015, pp. 687–692, doi: 10.1109/TSP.2015.7296351.

DMITRII SEMENOV is currently pursuing the degree with the Department of Radio Electronics, Faculty of Electrical Engineering and Communication, Brno University of Technology, Brno, Czech Republic. He is an Analog Design Intern with Semiconductor Supplier "Onsemi." His research interests include integrated analog circuits (active filters, operational amplifiers, and references), analog signal processing, circuit design based on operational transconductance amplifiers (OTA), and global optimization methods.

ROMAN SOTNER (Member, IEEE) was born in Znojmo, Czech Republic, in 1983. He received the M.Sc. and Ph.D. degrees in electrical engineering from Brno University of Technology, Brno, Czech Republic, in 2008 and 2012, respectively. Currently, he is an Associate Professor with the Department of Radio Electronics, Faculty of Electrical Engineering and Communication, Brno University of Technology. His research interests include discrete and integrated analog circuits (active filters, oscillators, and audio), circuits in the current mode, and circuits with direct electronic controlling possibilities, especially analog signal processing in sensing applications and computer simulation.

LADISLAV POLAK (Member, IEEE) was born in Štúrovo, Slovakia, in 1984. He received the M.Sc. and Ph.D. degrees in electronics and communication from Brno University of Technology (BUT), Czech Republic, in 2009 and 2013, respectively. He is currently an Associate Professor with the Department of Radio Electronics (DREL), BUT. His research interests include wireless communication systems, RF measurement, signal processing, and computer-aided analysis.

JAN JERABEK was born in Bruntal, Czech Republic, in 1982. He received the Ph.D. degree in electrical engineering from Brno University of Technology, Czech Republic, in 2011. He is currently an Associate Professor with the Department of Telecommunications, Faculty of Electrical Engineering and Communication, Brno University of Technology. His research interests include circuit integer-order and fractional-order design and the applications of modern active elements, such as adjustable current amplifiers and followers, transconductance, and trans-impedance amplifiers.

JIRI PETRZELA was born in Brno, Czech Republic, in 1978. He received the M.Sc. and Ph.D. degrees in the field of theoretical electronics, in 2003 and 2007, respectively. Currently, he is an Associate Professor with the Department of Radio Electronics, Faculty of Electrical Engineering and Communications, Brno University of Technology, Czech Republic. He is the main author or co-author of more than 30 journal articles and 40 international conference contributions. His research interests include numerical methods in electrical engineering, nonlinear dynamics, chaos theory, analog lumped circuit design, and computer-aided analysis.

LUKAS LANGHAMMER received the M.Sc. and Ph.D. degrees in electrical engineering and telecommunication from the Faculty of Electrical Engineering and Communication, Brno University of Technology (BUT), Brno, Czech Republic, in 2012 and 2016, respectively.

He is currently with the Department of Electrical Engineering, Faculty of Military Technology, University of Defence, Brno, and the Department of Telecommunications, Faculty of Electrical Engineering and Communication, BUT. His research interests include the design and analysis of frequency filters, basic analog building blocks, and advanced active elements.